International Journal of Fatigue 163 (2022) 107042

Contents lists available at ScienceDirect

International Journal of Fatigue

journal homepage: www.elsevier.com/locate/ijfatigue

The influence of welding heat input on Residual Notch Stress Intensity Factor

Paolo Ferro [a,*], Keke Tang [b], Filippo Berto [c]

[a] University of Padova, Department of Engineering and Management, Stradella S. Nicola, Vicenza, Italy
[b] School of Aerospace Engineering and Applied Mechanics, Tongji University, Shanghai 200092, China
[c] NTNU, Department of Engineering Design and Materials, Trondheim, Norway

ARTICLE INFO

Keywords:
Residual stress
Peak stress
Notch stress intensity factor
Welding
Steel
Fatigue strength

ABSTRACT

The influence of process parameters on the residual asymptotic stress distribution is investigated using a 3D numerical modeling of the welding process. Computational welding mechanics and the peak stress method are combined to calculate the residual Notch Stress Intensity Factors (R-NSIF) as a function of power input. Results are summarized in terms of heat input and discussed in view of a future guidelines proposal addressed to designers who are going to face a welding process optimization for fatigue life improvement.

1. Introduction

Residual stresses (RSs) are recognized to influence the fatigue strength of welded joints in the high cycle fatigue (HCF) regime [1–8]. Their value is tremendously influenced by a big number of parameters such as metallurgy of welded alloys [9,10], process parameters, boundary conditions and welding technology, among the others. This makes the comprehension of how residual stresses influence the HCF strength of welded joints very difficult and not completely understood yet. Some generally recognized findings are however well documented. For instance, it is well known that RSs do not influence the fatigue strength of weldments in medium and low cycle fatigue life regime. In this regard, Sonsino [8] emphasized the importance of local residual stresses and their redistribution during fatigue loading. Above the high cycle fatigue (HCF) range or variable amplitude loading, residual stresses do not show any evident effect on fatigue life. Thermal stress relief can be dropped, as – the author wrote – 'cyclic plastic deformation at the crack-like weld toes will have already eliminated the tensile residual stresses'. Again, Ferro et al. [11] demonstrated through numerical simulation that in the medium and low cycle fatigue regime the residual stress field ahead the weld toe completely redistributed after the first fatigue cycle, while it remained unchanged in the HCF regime. Basing on those observations, HCF life enhance techniques were developed, such as shot-peening or TIG-dressing [12,13], that are thought to switch the residual stresses at the weld toe from tensile to compressive. Both the above-mentioned techniques and attempts to include the residual stress effects on fatigue prediction criteria, presuppose the knowledge of residual stress fields. These can be conveniently predicted by a proper numerical simulation of the entire welding process. In literature, to avoid complicated fluid-dynamic phenomena simulations, computational welding mechanics (CWM) is used. The temperature history at each node is first assessed via a power density distribution function simulating the heat source moving over the welding line and then used as load for the mechanical computation. Solid-state metallurgical transformations are considered through constitutive equations of the alloy under investigation and their effect on residual stress value are calculated, as well. As soon as the residual stresses distribution is captured by numerical simulation, it can be considered in criteria for fatigue life estimation such as local approaches based on the Notch Stress Intensity Factor (NSIF) [14–16] or Averaged Strain Energy Density (ASED) parameters [17]. It is worth mentioning that the NSIF or ASED based criteria can be used to quantify the influence of RSs on fatigue strength of welded joints because it is demonstrated that the residual stress distribution ahead the weld toe is singular, in its nature, and follows the same features of external load-induced asymptotic stress distributions [18,19]. Because of the need of a fine mesh to capture the residual asymptotic stress fields, in previous works 2D models were used accepting the idea of losing information about the boundary effects. Today, with the development of rapid numerical techiques, such as the peak stress approach [20,21], it is possible to assess the residual NSIF (R-NSIF) using 3D modeling. This shortcut allows to investigate the effects

* Corresponding author.
E-mail address: paolo.ferro@unipd.it (P. Ferro).

https://doi.org/10.1016/j.ijfatigue.2022.107042
Received 2 March 2022; Received in revised form 25 May 2022; Accepted 27 May 2022
Available online 1 June 2022
0142-1123/© 2022 Elsevier Ltd. All rights reserved.

Nomenclature and Symbols

2α [°]	V-notch angle
a [mm]	Goldak's parameter linked to weld pool dimensions
b [mm]	Goldak's parameter linked to weld pool dimensions
C	Constant
c_1 [mm]	Goldak's parameter linked to weld pool dimensions
c_2 [mm]	Goldak's parameter linked to weld pool dimensions
d [mm]	Element size at weld toe
E [MPa]	Young's Modulus
e_I	Parameter (Mode I)
f_1	Constants for the energy distribution of the heat flux
f_2	Constants for the energy distribution of the heat flux
h [Wm^{-2} K^{-1}]	Convective heat transfer coefficient
HI [J/mm]	Heat Input
I [A]	Arc Welding Current
K^*_{FE}	Coefficient
k_I	Coefficiant (mode I)
K_I [MPa $mm^{0.326}$]	Notch stress intensity factor (Mode I), NSIF
l [mm]	Fusion zone width
Ms [T]	Initial martensite transformation temperature
p_i, p_j	Proportion of phases i and j, respectively
$p^{ij}_{jeq}(T)$	Equilibrium fraction of phase j at temperature T
p_m	Martensite proportion obtained at an infinitely low temperature
$p_m(T)$	Martensite proportion at temperature T
Q [W]	Power Input (V·I)
q_F [J/mm^3]	Frontal power density (Goldak heat source)
q_R [J/mm^3]	Rear power density (Goldak heat source)
Q_W [W]	Absorbed power
r [mm]	Cylindrical coordinate (Fig. 1a)
R-NSIF [MPa $mm^{0.326}$]	Residual Notch Stress Intensity Factor
R_C [mm]	Critical Radius
T [°C]	Temperature
t [mm]	Plate thickness
v [mm s^{-1}]	Welding speed
V [V]	Arc Welding Voltage
w [T^{-1}]	Constant
z	slope of fatigue data expressed in terms of local strain energy density
$\sigma_{\theta\theta,\theta=0,peak}$ [MPa]	Opening peak stress
τ_{ij} (T) [s]	Characteristic time of the transformation
$_{\Delta\sigma n}$ [MPa]	Nominal stress amplitude
η	Arc Welding Thermal Efficiency
$_{\lambda I}$	William's eigenvalue, with (1-λ_I) stress singularity exponent, mode I
$\sigma_{\theta\theta}$ [MPa]	θθ component of the stress, in the cylindrical coordinate system of Fig. 1a

of geometry, metallurgy [10] and process parameters on the R-NSIF distribution over the entire length of the bead, including therefore the boundary effects. In this work, authors focus their attention on the influence of power input on R-NSIF distributions induced by gas tungsten arc welding (GTAW) process applied to S355 structural steel.

2. Numerical model

A butt-welding process was simulated using Sysweld® code. The material is the S355 structural steel whose metallurgy, and its modelling, were described in a previous work [10]. The welding is supposed to be performed with only one pass. Taking advantage of the symmetry, only one half was modelled as shown in Fig. 1 where the global Cartesian and local cylindrical reference systems are displayed, as well.

33110 8-node brick elements were used to build the mesh, the smallest ones, in the vicinity of the weld toe, having a size (d) of 1 mm (Fig. 1b). It is noted that the weld toe profile is assumed to be a sharp V-notch with an angle (2α) of 135° and a null tip radius, i.e., the 'worst case' condition.

2.1. Thermal input

The heat generation due to the heat source moving over the weld line is described by the power distribution function proposed by Goldak et al. [22] for arc welding processes:

$$\begin{cases} q_F = \dfrac{6\sqrt{3}f_f Q_W}{abc_f\pi\sqrt{\pi}} \exp\left(\dfrac{-3x^2}{a^2}\right)\exp\left(\dfrac{-3y^2}{b^2}\right)\exp\left(\dfrac{-3z^2}{c_f^2}\right) & \text{source front} \\ q_R = \dfrac{6\sqrt{3}f_r Q_W}{abc_r\pi\sqrt{\pi}} \exp\left(\dfrac{-3x^2}{a^2}\right)\exp\left(\dfrac{-3y^2}{b^2}\right)\exp\left(\dfrac{-3z^2}{c_r^2}\right) & \text{source rear} \end{cases} \quad (1)$$

In previous expressions (1), q_F and q_R represent the frontal and rear power density, respectively; Q_W is the welding heat input estimated from the input current (I) and voltage (V) parameters ($Q_W = \eta VI$, with η the thermal efficiency set for GTAW equal to 0.7); f_f (=0.6) and f_r (=1.4) denotes the fractions of heat present in the front and rear parts of the heat source, while a, b, c_f and c_r are Gaussian parameters of the Goldak's heat source, as described in Fig. 2. Their values are in line with those

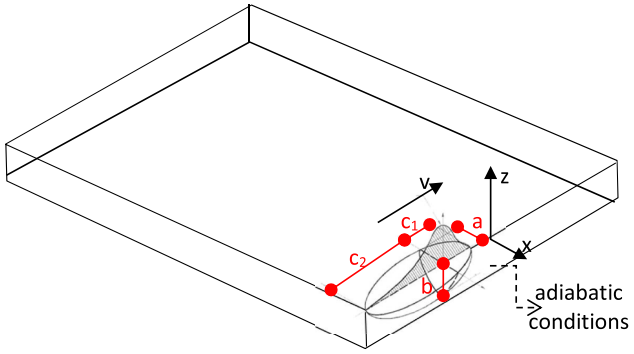

Fig. 2. Schematic of the geometrical parameters of the heat source.

used by the original paper by Goldak et al. [22], only slightly adjusted to achieve full penetration. Goldak's heat source parameters kept constant and adopted in the FE analyses have been summarized in Table 1, while those varied according to the analyzed trials have been collected in Table 2. Radiative and convective heat loss was modeled using the Stefan Boltzman Law and a convective heat transfer coefficient (h) equal to 25 Wm^{-2} K^{-1}, respectively.

A sequentially thermo-metallurgical/mechanical uncoupled simulation was carried out where a dedicated function was employed to set the

Table 1
Heat source parameters (*values varied according to Table 2).

Q	Power Input (V·I) [W]	*
η	Efficiency	0.7
Q_W	Absorbed power [W], with $Q_W = \eta Q$	–
a	Molten pool dimensions [mm]	0.5
b		3.5
c_1		0.5
c_2		3
f_1	Constants for the energy distribution of the heat flux	0.6
f_2		1.4
v	Welding speed [mm s^{-1}]	10

Table 2
Process parameters investigated.

Trial	Q [W]	v [mm s^{-1}]	Heat Input (Q*/v) (J/mm)
1	7300	10	511
2	8300	10	581
3	9300	10	651

mechanical properties of the material to zero in all nodes where the computed temperature was higher than the melting point (1500 °C). Moreover, isostatic clamping conditions were applied during and after welding.

2.2. Peak stress method applied to residual stresses

In local approaches, the weld toe is schematized, referring to the worst case, as a sharp V notch, zero tip radius, inducing an asymptotic stress field whose intensity is quantified by the NSIF, K_I, given by Gross and Mendelson's definition [23] as follows (2):

$$K_1 \cong \sqrt{2\pi}\cdot\lim_{r\to 0}[(\sigma_{\theta\theta})_{\theta=0}\cdot r^{1-\lambda_1}] \quad (2)$$

where the linear elastic local stress component $\sigma_{\theta\theta}$ of the stress field is calculated near the weld toe ($r \to 0$) and along the notch bisector line ($\theta = 0$), as sketched in Fig. 1a, while the parameter ($1-\lambda_I$) is the stress singularity exponent, which equals 0.326 for $2\alpha = 135°$.

When considering RSs, the NSIF is called R-NSIF. A rapid technique used to calculate it, even by means of 3D numerical models, is the Peak Stress Method (PSM). It allows for the estimation of NSIFs and R-NSIFs starting from the opening peak stress, $\sigma_{\theta\theta,\theta=0,peak}$, calculated at the V-notch tip with a coarse mesh (Fig. 1b), according to:

$$K_1 \cong K^*_{FE}\cdot\sigma_{\theta\theta,\theta=0,peak}\cdot d^{1-\lambda_1} \quad (3)$$

where d is the average element size adopted to mesh the weld toe (d = 1 mm, in this work). The coefficient K^*_{FE} was calibrated elsewhere [21] and the value obtained is 1.64 ± 5%. It is worth mentioning that, through convergence analysis, d = 1 mm was found in a previous work [21] to be the largest element size providing at the same time a correct value of thermal gradients and R-NSIF. Moreover, due to the simple welded joint geometry, a mapped mesh was used as shown in Fig. 1b. However, it was demonstrated [21] that 10-node tetra elements can be used as well allowing the use of free meshing more suitable to complex geometries. Also in this case, the best value of d was equal or lower than 1 mm [21].

3. Results and discussion

3.1. Thermo-metallurgical results

Fig. 3 shows the fusion zone (FZ) produced by the heat source during welding as a function of power input (Q). It is worth mentioning that the bead geometry was adapted according to the analyzed process parameters. The higher the heat input the larger the weld bead. As a matter of fact, the bead geometry varies with process parameters so that it was necessary to modify the dimension (l(HI) in Fig. 1a) of the fusion zone since fluid dynamic phenomena are not simulated in CWM approach.

Diffusion-controlled phase transformations are modelled by means of the Leblond– Devaux [24] equation:

$$\dot{p_j} = \frac{p^{ij}_{jeq}(T) - p_j}{\tau^{ij}(T)} \quad (4)$$

where p_i and p_j denote the proportion of phases i and j, respectively ($p_i + p_j = 1$); $p^{ij}_{jeq}(T)$ is the equilibrium fraction of phase j at temperature T, τ_{ij} (T) represents the characteristic time of the transformation (at constant temperature T, p_j tends exponentially towards $p^{ij}_{jeq}(T)$ with a time constant equal to τ_{ij} (T)). Martensitic transformation is modelled by means of the Koistinen–Marburger law [25]:

$$p_m(T) = p_m(1 - \exp(-w(Ms - T))) \quad (5)$$

where p_m is the phase proportion obtained at an infinitely low temperature (p_m is frequently assimilated to 1), and Ms and w characterize the initial transformation temperature and the evolution of the transformation process according to the temperature, respectively. Finally, phases proportion is calculated at each node by using equations (4) and (5), temperature value and its time derivative.

Regarding the S355 steel microstructure, it is observed (Fig. 4) that the FZ is characterized by a mixture of bainite and ferrite, with an increase of ferrite as the power input increases. This is due to a decrease of cooling rate with the increase of the power input. Moreover, a stationary distribution of the microstructure is observed along the central part of the joint.

3.2. Mechanical results and discussion

Fig. 5 shows the R-NSIF distribution along the entire weld toe and induced by the welding trial 1 (Table 2).

It is observed how the R-NSIF distribution is characterized by high variations near the boundaries and a plateau far from them. Such

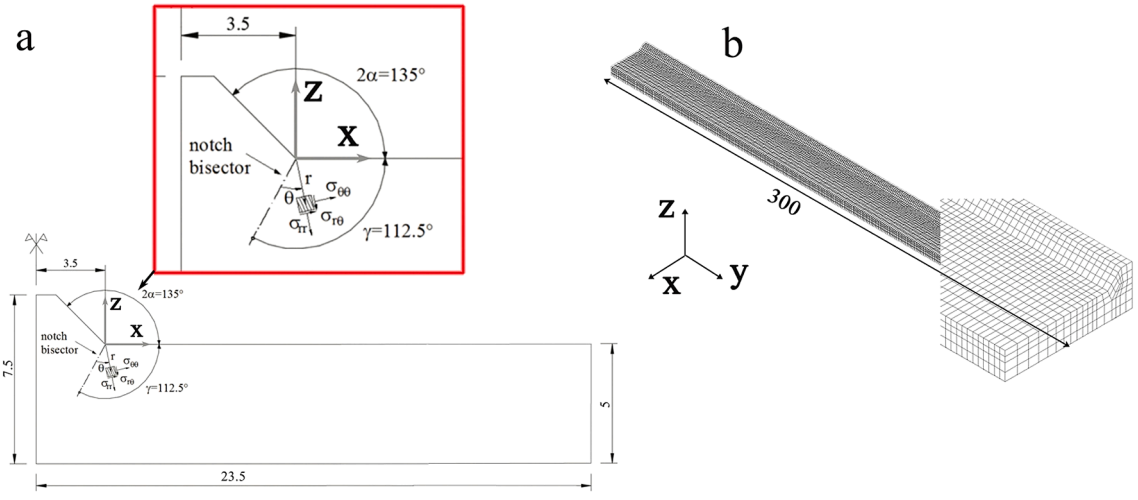

Fig. 1. (a) Geometry of a cross section with local cylindrical coordinate system and (b) 3D numerical model of the butt-welded joint [mm]. l(HI) is the FZ width that is a function of the heat input (HI) (dimensions in mm).

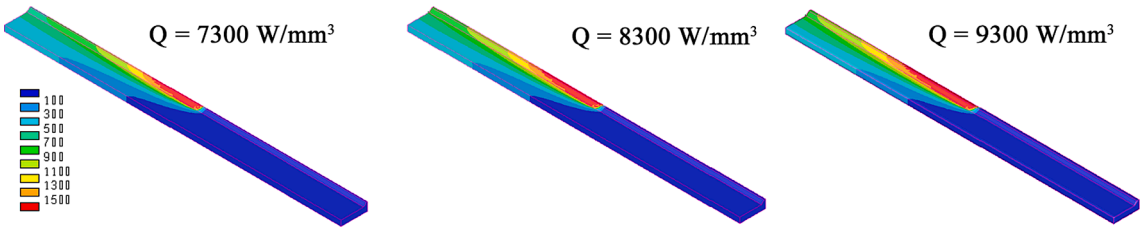

Fig. 3. Temperature map after 15 s from welding start as a function of power input (Q).

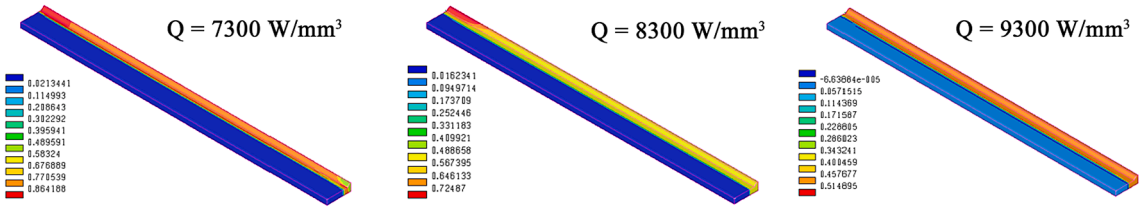

Fig. 4. Bainite proportion at room temperature after welding.

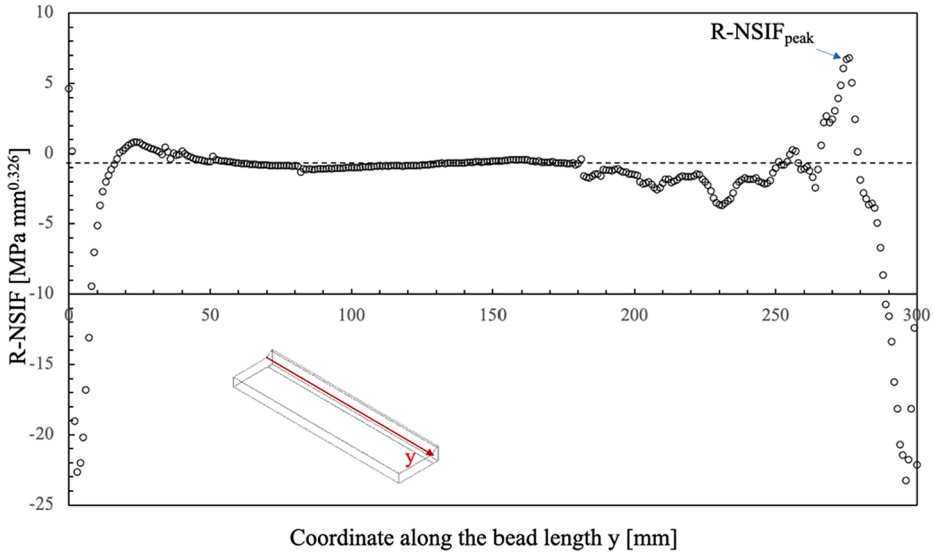

Fig. 5. R-NSIF distribution along the weld bead.

stationary value is the same that is captured by 2D models, as demonstrated in a previous work [26]. The 3D modeling highlights therefore the boundaries effects that seem more dangerous (in terms of high values of R-NSIF) compared to the stationary R-NSIF distribution. Different boundary effects are observed at the source input zone (compared to those that arose in the heat source output zone) reflecting the non-symmetric microstructure proportion at the boundaries induced by welding. Fig. 6 shows the R-NSIF value at the middle section of the specimen as a function of the heat input. It is interesting to note that a non-monotonic trend was found that can be justified by a strong interaction between geometry (weld bead size variations) and thermo-metallurgical history the joint undergoes for each different welding process combination. Fig. 7 shows schematically such intriguing interaction.

The heat input influences the heating and cooling rate in FZ and HAZ, and therefore the resulting microstructure. The lower the heat input, the higher the cooling rate and the percentage of acicular more resistance phases in terms of yield strength and ultimate tensile strength (i.e.: bainite or martensite) compared to allotriomorphic and weaker microstructures (i.e.: ferrite, pearlite). At the same time, the higher the cooling rate, the lower the temperature interval transformation and the higher the specific volume variation (Fig. 8) as well as transformation plasticity effects. Bainite, in particular, is the result of displacive austenite to ferrite transformation while carbon diffuses to produce carbides higly dispersed within the ferritic matrix. This acicular and very fine microstructure is characterized by high strength and toughness according to the well-known Hall-Petch law. Depending on geometry and boundary conditions, such metallurgical effects may reduce or increase the residual stress near the weld toe [9]. Finally, the heat input modifies the weld bead geometry (Fig. 7); the higher the heat input the higher the FZ and HAZ dimensions. In this work, it is supposed that V-notch angle at the weld toe keeps constant, while the width of FZ (l(HI) in Fig. 1a) increases accordingly to the heat input. This means that the ratio l(HI)/L increases with the HI inducing a reduction of R-NSIF [26]. Because of all the above-mentioned interacting effects, it is a difficult task to find a generalized heat-input/residual stress trend. Thus, each combination material-geometry-process parameters should be studied as a separate case.

To find a correlation between heat input and fatigue strength (FS) of welded joints is even more challenging since the interaction among different effects is even more complicated (Fig. 7). The HI influences the geometry that in turn affects the FS both directly (size effect) and

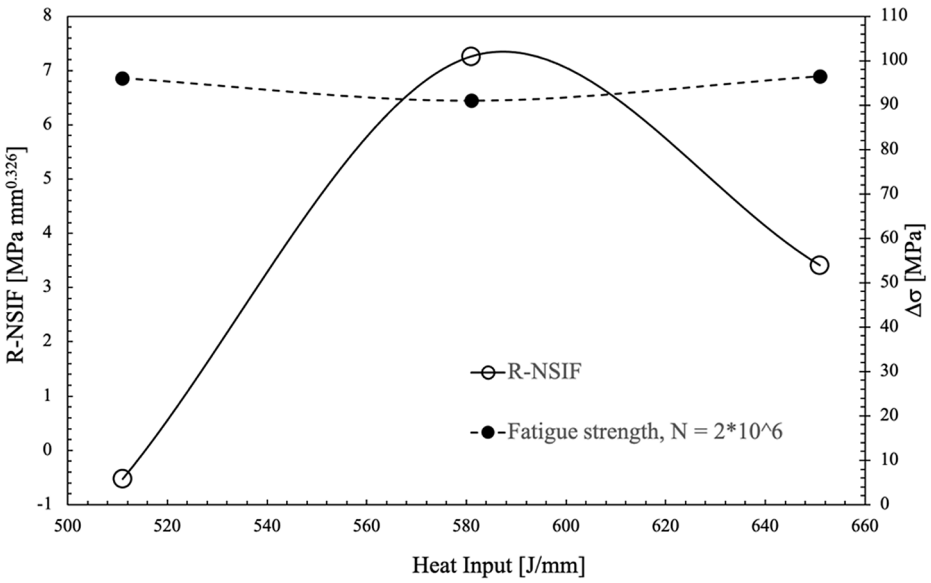

Fig. 6. R-NSIF value at the middle section of the joint and predicted fatigue strength Δσ (at 10^6 cycles) as a function of the heat input.

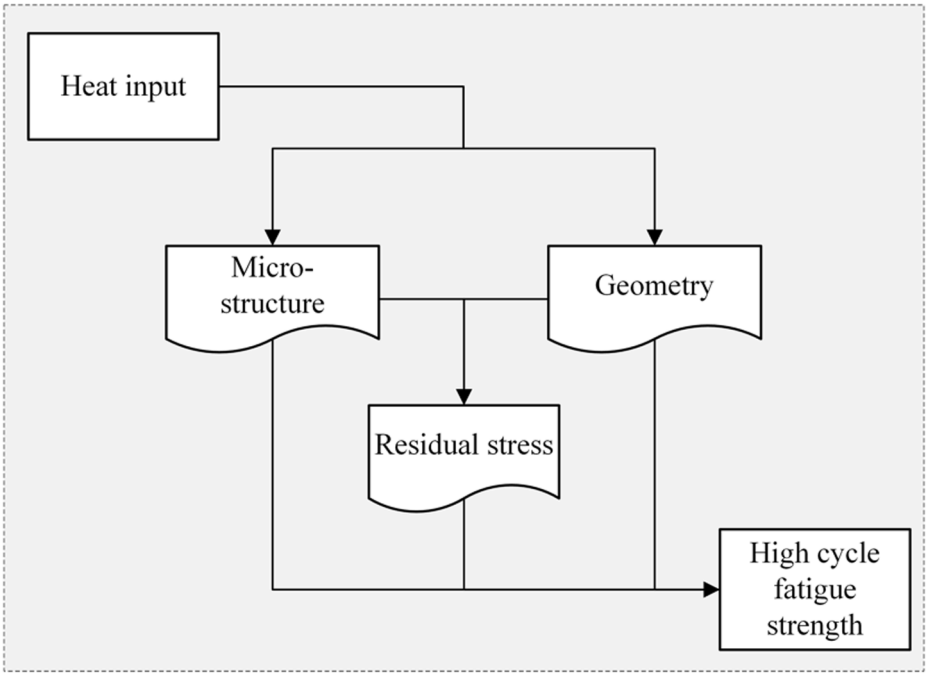

Fig. 7. Interaction phenomena among heat input, residual stress, and high cycle fatigue strength of a welded joint.

indirectly, through the variation of the residual stress [26]. In the same way, the HI influences the microstructure that in turn affects the fatigue strength both directedly (the higher mechanical properties, the higher the fatigue strength of alloys) and indirectly, through the variation of the residual stress (the lower the transformation temperature interval, the higher the specific volume variation (Fig. 8) and the resulting residual stress). For this reason, in the attempt to find a generic correlation between heat input and fatigue strength of welded joints, contradictory results were found in literature. In their investigation on the effect of heat input in mechanical and metallurgical properties of welds made of advanced high strength steel joined with gas metal arc welding (GMAW) process, Lopez et al. [27] found no influence in the low cycle regime (LCR), where plastic effects at the weld toe completely redistribute the pre-existing residual stresses; while the higher the heat input, the higher the fatigue strength in the high cycle regime (HCR) of the investigated samples, even if such variation was very low. Similar results were obtained in a recent work by Hassan et al. [28]. They found that the fatigue limit at 10^7 cycles of welded joints made of low carbon steel AISI 1020, had a negligible variation of about 3 MPa with a variation of the HI of 300 J/mm. Chang et al. [29] showed that the high heat input did not cause the degradation in fatigue crack propagation of their welded joints made of conventional steel. On the contrary, but with a completely different welded joint geometry (double-sided fillet welds made of S460MC steel), Moravec et al. [30] found a significant variation in the fatigue strength at HCR induced as a function of HI. The higher the heat input, the lower the high cycle fatigue strength. It is well recognized that residual stress is one of the main parameters affecting the fatigue strength of welded joints [31,32]. On the other hand, residual stress is

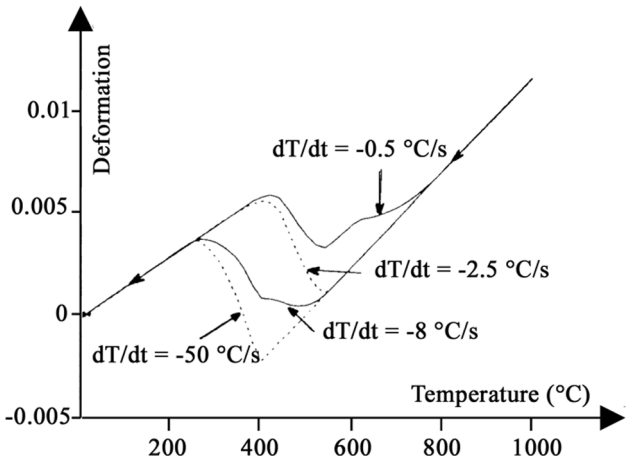

Fig. 8. Dilatometric curve of a steel as a function of cooling rate (dT/dt).

affected by the HI as shown in Fig. 6 and reported by other authors in literature [33]. In this scenario, the R-NSIF values calculated as a function of HI, can be used to predict the influence of residual stress on the fatigue strength of welded joints in the high cycle regime using Eq. (6) [17]:

$$\Delta\sigma_n = \frac{R_C^{1-\lambda_I}\left[\frac{E}{e_I}\left(\frac{C}{N}\right)^{1/z}\right]^{1/2}}{k_I t^{1-\lambda_I}} - \frac{(R-NSIF)_{peak}}{k_I t^{1-\lambda_I}} \quad (6)$$

where $\Delta\sigma_n$ is the nominal stress amplitude, E is the elastic modulus, C is a constant and z is the slope of the fatigue data expressed in terms of experimentally calculated local strain energy density; t is the plate thickness, k_I is a non-dimensional coefficient, analogous to the shape functions of cracked components. R_C is a material constant which represents the critical radius of a circular sector, centered on the notch tip, over which the strain energy density is averaged. Finally, e_I is a parameter which depends on V-notch opening angle (2α), Poisson's ratio (υ) and the failure hypothesis adopted. Results obtained with Eq. (6) are shown in Fig. 6, which shows a negligible variation of the fatigue strength at HCR due to the very low value of R-NSIF$_{peak}$ derived from the geometry and process parameters used in the numerical analysis of the present work. This is also confirmed by above cited literature works as well as the numerical and experimental work by Suh et al. [34].

4. Conclusions

The R-NSIF as a function of power input was assessed via numerical simulation. Solid-state phase transformations as well as weld bead geometry variations were considered. The obtained results showed a stationary value of the R-NSIF in the middle zone of the bead which reflects a stationary thermo-metallurgical history the joint undergoes during welding. Boundary effects were captured, as well, that seem more dangerous than the stationary field-characterized zone. A non-monotonic trend was captured between the heat input and the R-NSIF value that is the result of a strong interaction between the geometry (weld bead size variations induced by process parameters variations) and thermo-metallurgical history. Finally, the high cycle fatigue strength of the analyzed welded joints was estimated using a model already published in literature (Eq. (6), [17]). Because of the law variation of R-NSIF as a function of heat input, a negligible variation of the fatigue strength was (consequently) predicted that confirms different experimental results found in literature.

Declaration of Competing Interest

The authors declare that they have no known competing financial interests or personal relationships that could have appeared to influence the work reported in this paper.

References

[1] Krebs J, Kaßner M. Influence of welding residual stresses on fatigue design of welded joints and components. Weld World 2007;51(7):54–68.
[2] Klassen J, Friedrich N, Fricke W, Nitschke-Pagel T, Dilger K. Influence of residual stresses on fatigue strength of large-scale welded assembly joints. Weld World 2017;61(2):361–74.
[3] Fricke W, von Lilienfeld-Toal A, Paetzold H. Fatigue strength investigations of welded details of stiffened plate structures in steel ships. Int J Fatigue 2012;34(1):17–26.
[4] Tremarin RC, Pravia ZMC. Analysis of the Influence of Residual Stress on Fatigue Life of Welded Joints. Latin Am J Solids Struct 2020;17(3):e262.
[5] Lopez-Jauregi A, Esnaola JA, Ulacia I, Urrutibeascoa I, Madariaga A. Fatigue analysis of multipass welded joints considering residual stresses. Int J Fatigue 2015;79:75–85.
[6] Bae D, Sohn I, Hong J. Assessing the effects of residual stresses on the fatigue strength of spot welds. Weld J 2003;82:18–23.
[7] Shen W, Yan R, Wang X, Liu E, Xu L. Fatigue life evaluation of welded joints considering the local multiaxial stress/strain states and numerically determined residual stresses/strains. Int J Steel Struct 2017;17(1):139–53.
[8] Sonsino CM. Effect of residual stresses on the fatigue behavior of welded joints depending on loading conditions and weld geometry. Int J Fatigue 2009;31:88–101.
[9] Ferro P. The influence of phase transformations on the asymptotic residual stress distribution arising near a sharp V-notch tip. Model Simul Mater Sci Eng 2012;20(8):085003.
[10] Ferro P, Berto F, Bonollo F, Tang K. Does metallurgy affect the residual notch stress intensity factor value induced by welding operations? A comprehensive study via a 3D numerical model. Int J Fatigue 2021;149:106261.
[11] Ferro P, Berto F, James NM. Asymptotic residual stresses in butt-welded joints under fatigue loading. Theor Appl Fract Mech 2016;83:114–24.
[12] Huo L, Wang D, Zhang Y. Investigation of the fatigue behaviour of the welded joints treated by TIG dressing and ultrasonic peening under variable-amplitude load. Int J Fatigue 2005;27(1):95–101.
[13] van Es SHJ, Kolostein MH, Pijpers RJM, Bijlaard FSK. TIG-dressing of high strength steel butt welded connections – Part 1: weld toe geometry and local hardness. Procedia Eng 2013;66:216–25.
[14] Williams ML. Stress singularities resulting from various boundary conditions in angular corners of plates in extension. J Appl Mech 1952;19:526–8.
[15] Rice JR, Rosengren GF. Plane strain deformation near a crack tip in a power-law hardening material. J Mech Phys Solids 1968;16(1):1–12.
[16] Hutchinson JW. Singular behavior at the end of a tensile crack in a hardening material. J Mech Phys Solids 1968;16:13–31.
[17] Ferro P. The local strain energy density approach applied to pre-stressed components subjected to cyclic load. Fatigue Fract Eng Mater Struct 2014;37(11):1268–80.
[18] Ferro P, Berto F, Lazzarin P. Generalized stress intensity factors due to steady and transient thermal loads with applications to welded joints. Fatigue Fract Eng Mater Struct 2006;29(6):440–53.
[19] Ferro P, Petrone N. Asymptotic Thermal and Residual Stress Distributions due to Transient thermal Loads. Fatigue Fract Eng Mater Struct 2009;32(11):936–48.
[20] Meneghetti G, Campagnolo A. State-of-the-art review of peak stress method for fatigue strength assessment of welded joints. Int J Fatigue 2020;139:105705.
[21] Campagnolo A, Ferro P, Romanin L, Meneghetti G. Residual Notch Stress Intensity Factors in Welded Joints Evaluated by 3D Numerical Simulations of Arc Welding Processes. Materials 2021;4(4):812–32.
[22] Goldak J, Chakravarti A, Bibby M. A new finite element model for welding heat source. Metall Trans B 1984;15B:299–305.
[23] Gross B, Mendelson A. Plane elastostatic analysis of V-notched plates. Int J Fract Mech 1972;8(3):267–76.
[24] Leblond JB, Devaux J. A new kinetic model for anisothermal metallurgical transformations in steels including the effect of austenite grain size. Acta Metall 1984;32:137–46.
[25] Koistinen DP, Marburger RE. A general equation prescribing extent of austenite–martensite transformation in pure iron–carbon alloys and carbon steels. Acta Metall 1959;7:59–68.
[26] Ferro P. Is 2D numerical modelling of welding process able to capture the residual notch stress intensity factor values? Theor Appl Fract Mech 2021;114:103006.
[27] Lopez V, Reyes A, Zambrano P. Effect of the heat input in the mechanical and metallurgical properties of welds on AHSS transformed induced plasticity steel joined with GMAW process. In: The 2013 Word Congress on Advances in Structural Engineering and Mechanics (ASEM13). Jeju, Kprea, September 8-12; 2013.
[28] Hassan KS, Fayyadh SK, Dhayea A. Fatigue Life of Welded Joint Improvement with Various Welding Principles and Shot Peening process for AISI 1020 Low Carbon Steel. J Mech Eng Res Develop 2021;44(4):221–32.
[29] Chang RW, Kweon YG, Lim CB. Influence of Welding Heat Input On Fatigue Crack Propagation Behavior Of Offshore Structural Steels Welds. First ISOPE Pacific/Asia Offshore Mechanics Symposium, Seoul, Korea; June 1990.
[30] Moravec J, Sobotka J, Solfronk P, Thakral R. Heat Input Influence on the Fatigue Life of Welds from Steel S460MC. Metals 2020;10:1288–302.
[31] Nelson DV. Effect of residual stress on fatigue crack propagation, residual stress effects in fatigue. ASTM STP 1982;776:172–4.

[32] Chongmin K, Diesburg DE. Effect of residual stress on fatigue fracture of case-hardened steels - an analytical model, residual stress effects in fatigue. ASTM STP 1982;776:224–34.
[33] Chang PH, Teng TL. Numerical and experimental investigations on the residual stresses of the butt-welded joints. Comput Mater Sci 2004;29(4):511–22.
[34] Suh CH, Lee RG, Oh SK, Jung Y-C, Son J-Y, Kim YS. Effect of welding heat input on fatigue life of quenched boron steel and FB steel lap joint. J Mech Sci Technol 2011;25(7):1727–35.